




## A comparative analysis of curvilinear configurations of the V-dipole antenna

Ayotunde A. Ayorinde , Sulaiman A. Adekola , Ike Mowete 

University of Lagos  
University Road,  
Lagos, Nigeria

**Abstract – Background.** Curvilinear dipole antenna structures have been established as solution to the directivity problem associated with conventional dipole antennas, with length greater than half a wavelength. However, with the exception of the ‘concave Nu’ dipole, other curvilinear configurations of V-dipole antenna have yet to receive analytical attention in the open literature. This paper presents a comparative analysis of four of such configurations. **Aim.** Develop a detailed electric field integral equation formulation for internal electrodynamic problem of four curvilinear configurations of the V-dipole antenna structure, such that a method of moments solution becomes applicable. **Methods.** Unknown current distributions in the formulation are determined using the method of moments, with piece-wise linear basis and testing functions. Analytical results are then implemented in a FORTRAN computer program, for numerical results. **Results.** Analytical models for four curvilinear configurations of the V-dipole antenna as well as computational results for their input and radiation-zone characteristics. **Conclusion.** Computational results obtained reveal that in terms of maximum achievable directivity and return loss, the configuration with both arms curved, is the best performing; followed by the conventional-V, convex-Nu (one arm bent inwards), and concave-Nu (one arm bent outwards), in that order.

**Keywords –** curvilinear dipole antenna; maximum directivity; moment-method; Nu dipole antenna configurations; return loss.

### Introduction

One notable limitation of the linear dipole antenna as identified in the literature, is that when its physical length exceeds half a wavelength at the operating frequency, its directivity profile deteriorates significantly. According to [1; 2], this limitation owes mainly to the fact that as its length increases, current distribution along the axis of the antenna will include components in direct phase opposition; with the consequence that directivity decreases significantly. Indeed, as remarked by [3], when the physical length is greater than one wavelength, the linear dipole’s main lobe resolves into a number of lobes of about equal strengths, which is why in practical applications, electrically shorter linear dipoles are preferred, despite their low gain features.

As a means of moderating the influence of undesirable phase characteristics of the current distributions of longer linear dipole antennas (LDA), [1; 2], in what appear to be pioneering contributions, introduced the idea of ‘shaping’ the LDA to form what is now commonly referred to as the ‘shaped dipole’. In particular, and starting with a geometry defined by piece-wise linear wires, in which each segment is inclined at some angle to the vertical, a shape that provided the largest value of maximum antenna effective height (and hence, directivity), was derived in [2].

The COMSOL-supported investigations reported in [3] highlighted the possibility of simultaneously optimizing both impedance and directivity of the wire antenna, and reported results that support the conclusion in [1; 2] concerning the ‘shaped dipole’. This ‘shaped dipole’, which, due to its similarity to the Gaussian (normal) probability distribution curve, has been named the ‘Gauss Dipole’, [4; 5], informed quite a few investigations into the characterizing features of curvilinear wire antennas [3–8]. Majority of these investigations focused on antenna directivity maximization, typically, through the use of arrays of the Gauss dipole. For example, after establishing through a moment-method / simplex optimization scheme that the  $3\lambda/2$  Gauss-shaped dipole represented the optimum (in terms of maximum directivity), [6], the same authors, in [7], analytically demonstrated that the 11,8 dB maximum directivity of a 3-element Yagi-Uda of dipole is almost identical to the experimentally determined value reported in [2]. A contribution by [8] addressed the problem of optimizing sidelobe level (SLL), using the example of a 6-element Yagi-Uda array of Gauss dipoles. The paper’s results suggested that maximum directivity achievable with SLL optimization is about 1,35 dB less than that achievable, when only directivity is optimized. It is noteworthy that in the case of [4], where the Gauss-dipole’s front-to-back ratio (FBR)

optimization problem was investigated, a gain of 12,87 dB was reported for a Gauss-dipole, backed by a square-shaped, finite-sized reflector. Results published in [9] also demonstrated that further improvements in the Gauss Dipole's performance (effective height in this case) can be achieved through the introduction of a geometrical asymmetry into the antenna's structure.

Outcomes of investigations concerning the 'arc-shaped' antenna described in [10; 11], appear to support the remark in [12] that curvilinear wire antennas are generally better performing than linear wire antenna structures. And according to [12], the V-dipole antenna (VDA) represents 'a first approximation' to the general class of curvilinear wire antennas. Results of a comparison of the performances of V- and Gauss-dipole antennas in [5] indicated that whereas, the maximum achievable directivities for both antennas are comparable, the Gauss-dipole is the better of the two. It is instructive to observe that despite being regarded as the 'optimum shaped curvilinear antenna' in the literature [1–7], no practical application of the Gauss-dipole antenna has, as far as can be ascertained, been reported. On the other hand, a number of important practical applications for the VDA have been highlighted in the literature. The more notable of these include the design of ultra-thin plasmonic meta-surfaces, [13], ground penetrating radar (GPR) applications, [14], and Ultra-Wideband applications [15]. As may be expected therefore, a number of schemes for the performance improvement of the VDA have been developed [5; 14; 16; 17]. An example is available from [14], which described the use of resistive loading along the antenna's arms to obtain pencil-beam patterns, utilized by GPR applications. Other examples include the performance optimization schemes involving choice of arm configuration and apex angle, explored in [16; 17].

This paper's main interest is in the investigations described in [5; 16; 17], which demonstrated that certain configurations of the VDA offer better performance possibilities than the conventional VDA. A configuration of particular interest is the curvilinear 'Nu-dipole' geometry treated by [18], in which the lower arm of the antenna takes the shape of an arc of a circle. Although [18] made no explicit performance comparisons between the VDA and Nu-dipole antenna, results presented in [16] for the 'arc-curved' dipole (with both lower and upper arms shaped as arcs of circles) clearly suggested that the arc-curved dipole provided a better 'maximum peak

radiated pulse' than the VDA, when both are shape-optimized. In this paper, three different curvilinear configurations of the VDA (the 'Nu' with lower arm curved inwards, the 'Nu', with lower arm curved outwards, and the 'Nu' with both arms curved in the same direction) are considered for performance comparisons, in terms of directivity, input impedance, return loss, and radiation-zone fields. Computational results reveal that in terms of these performance metrics, the 'Nu' with both arms curved in the same direction performs best with a maximum directivity greater than 8 dB, for example, when total dipole length is  $5\lambda/2$ . Computational results also suggest that a particularly notable consequence of shaping the arms of the dipole in a vee-configuration is the significant redistribution of the phase of current flow, along the antenna's axis. The paper in section 1, presents the theoretical background for the investigations, while computational results are presented and discussed in section 2. Suggestions for the extension of the work as well as the main conclusions due to the investigations are presented in section 3, the paper's concluding section.

## 1. Analysis

A useful approach to antenna analysis derives for example, from the observation by Tabakov and Al-Nozaili, [19], that the associated electrodynamics problem consists of two distinct, but very closely related component parts. First is the 'internal problem', whose solution prescribes the antenna's current distribution; and second is the 'external problem', through which the properties of the electromagnetic field due to the current distribution, are determined. One method of formulating this generic problem is to develop an electric field integral equation (EFIE), typically, with the use of three steps. In the first step, boundary conditions on the electric field at the surface of the antenna are imposed, followed in the second step, by the specification of the fields in terms of the Lorentz potentials. These potentials, in the last step, are described by the current and charge distributions associated with the antenna, as their sources. When this formulation is in the frequency domain (with an assumed  $e^{j\omega t}$  harmonic time variation), the most widely used integral equation is the 'two potential' equation, [20], essentially because compared with Pocklington's and Schelkunoff's equations (both of which also derive from the boundary conditions) its kernel is easier to handle.

In the case of the assumedly perfectly conducting, thin-wire antennas of particular interest here, these formulation steps are summarized by the following expressions:

$$\hat{\mathbf{a}}_N \times (\mathbf{E}_{imp} + \mathbf{E}_w) = 0, \text{ on } S \quad (1)$$

so that

$$-\mathbf{E}_{imp}^{\tan} = -j\omega\mathbf{A} - \frac{\partial\Phi}{\partial l} \hat{\mathbf{a}}_l, \text{ on } S \quad (2)$$

provided that

$$\mathbf{A} = \frac{\mu}{4\pi} \int_{axis} \mathbf{I}(l') \frac{e^{-jkR}}{R} dl', \quad (2a)$$

with

$$\Phi = \frac{1}{4\pi\epsilon} \int_{axis} \sigma(l') \frac{e^{-jkR}}{R} dl'. \quad (2b)$$

In the foregoing expressions,  $(\hat{\mathbf{a}}_N, \hat{\mathbf{a}}_l)$  represent unit vectors normal to the wire surface (in the outward direction) and in a direction tangential to the surface, respectively; while all other symbols retain their usual meanings. By relating filamentary charge and current distributions through the equation of continuity according to

$$\sigma(l') = -\frac{1}{j\omega} \frac{dI(l')}{dl'}, \quad (3)$$

the desired EFIE emerges through the use of (3) in (2b) and subsequent use of (2a) and (2b) in (1), in terms of the current distribution (and its first derivative), and constitutes the internal electrodynamic problem, [19], for the generic thin-wire antenna problem.

Towards a moment-method solution of the problem, a linear integro-differential operator, 'L' is introduced, [20], such that the EFIE modifies to

$$\mathbf{E}_{imp}^{\tan} = L[\mathbf{I}(l')] = (j\omega\mathbf{A} + \nabla\Phi)^{\tan} \text{ on } S. \quad (4)$$

It may be remarked that the domain of  $L$  is the space of those functions  $\mathbf{I}$ , for which  $\mathbf{I}$  is 0 at the ends of the wire antenna; and its range is the space of all possible functions  $\mathbf{E}_{imp}^{\tan}$  on the wire surface. An inner product  $(\langle \cdot \rangle)$  appropriate to the problem is also introduced for two vector quantities  $(\mathbf{W}, \mathbf{F})$  tangential to the wire surface as

$$\langle \mathbf{W}, \mathbf{F} \rangle = \int_C \mathbf{W} \cdot \mathbf{F} dl, \quad (5)$$

where 'C' is a path defined on the surface of the wire, parallel to its axis. Next, a set  $\{\mathbf{F}_n\}_{n=1}^N$  of expansion functions as well as a set  $\{\mathbf{W}_m\}_{m=1}^N$  of weighting functions are selected. Details of the requisite prop-

erties of these functions are available in [21; 23]. The unknown current distribution is then expressed as a series in terms of the expansion functions; that is:

$$\mathbf{I} = \sum_n \varsigma_n \mathbf{F}_n$$

in which the  $\varsigma_n$  are unknown coefficients to be determined. Equation (4) then modifies to

$$\sum_n L[\varsigma_n \mathbf{F}_n] = (j\omega\mathbf{A} + \nabla\Phi)^{\tan} = \mathbf{E}_{imp}^{\tan}, \quad (6)$$

so that by taking the inner product of each  $\mathbf{W}_m$  with both sides of (6), the system of equations defined by

$$\sum_n \langle \mathbf{W}_m, \varsigma_n L[\mathbf{F}_n] \rangle = \langle \mathbf{W}_m, \mathbf{E}_{imp}^{\tan} \rangle, \quad (7)$$

emerges. The matrix format of (7) is obtained through the definition of generalized network parameters according to, [21],

$$[Z] = \begin{bmatrix} \langle \mathbf{W}_1, L(\mathbf{F}_1) \rangle & \dots & \langle \mathbf{W}_1, L(\mathbf{F}_N) \rangle \\ \dots & \dots & \dots \\ \langle \mathbf{W}_N, L(\mathbf{F}_1) \rangle & \dots & \langle \mathbf{W}_N, L(\mathbf{F}_N) \rangle \end{bmatrix},$$

$$(V) = \begin{pmatrix} \langle \mathbf{W}_1, \mathbf{E}_{imp}^{\tan} \rangle \\ \vdots \\ \langle \mathbf{W}_N, \mathbf{E}_{imp}^{\tan} \rangle \end{pmatrix}, \text{ and } (I) = \begin{pmatrix} \varsigma_1 \\ \vdots \\ \varsigma_N \end{pmatrix},$$

such that (7) becomes

$$[Z](I) = (V).$$

It is of interest to observe, as shown in [22], that a typical entry to the generalized impedance matrix  $[Z]$  is of the form

$$Z_{mn} = \quad (8)$$

$$= \int_{axis} dl \int_C dl' \left( j\omega\mu \mathbf{W}_m \cdot \mathbf{F}_n + \frac{1}{j\omega\epsilon} \frac{dW_m}{dl'} \frac{dF_n}{dl} \right) \frac{e^{-jkR}}{4\pi R}.$$

Thus, the solution to the internal electrodynamic problem is obtained as

$$(I) = [Z]^{-1}(V). \quad (9)$$

### 1.1. Specialization to the curvilinear dipole cases

The illustrations of Fig. 1 describe the four configurations of the V-dipole antenna (VDA) considered in this paper. Fig. 1, *a*, depicts a curvilinear configuration with its lower arm curved inwards and here referred to as the 'concave-Nu'; Fig. 1, *b*, is for the 'convex-Nu', with lower arm curved outwards; Fig. 1, *c*, the 'conventional Nu', with both arms curved in the same direction; and Fig. 1, *d*, describes the VDA.

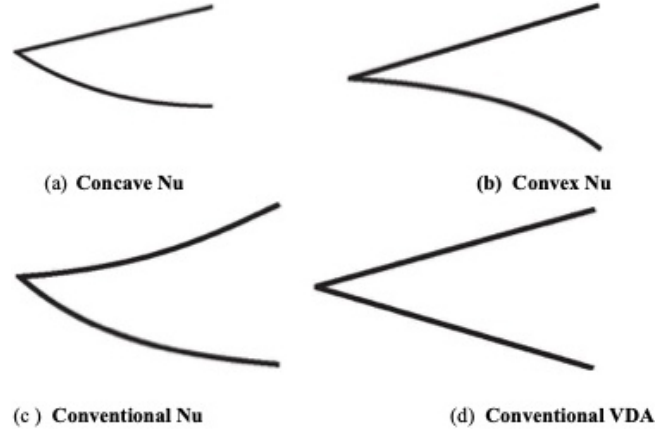


Fig. 1. Curvilinear configurations of the V-dipole antenna

Рис. 1. Криволинейные конфигурации V-дипольной антенны

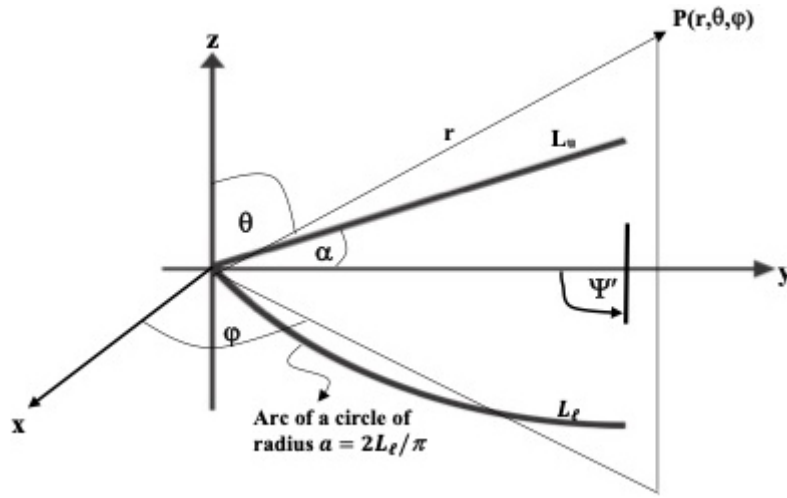


Fig. 2. Representative problem geometry

Рис. 2. Типичная геометрия задачи

Towards specializing the results of the foregoing discussions to the internal electrodynamic problem of these curvilinear configurations, the representative problem geometry of Fig. 2, for the ‘concave nu-dipole’ is considered. As a matter of analytical convenience, the dipole is regarded as consisting of two wires (an ‘upper arm’ and a ‘lower arm’) sharing a common feed.

For this ‘two-wire structure’, two sets of expansion and weighting functions are defined for the upper and lower arms according to

$$\left[ \{F_{u,n}\}; \{W_{u,m}\} \right] \text{ and } \left[ \{F_{l,n}\}; \{W_{l,m}\} \right],$$

respectively. Current distribution along the axes of the antenna structure is then given by

$$\mathbf{I} = \sum_{n=1}^{N/2} \varsigma_{u,n} \mathbf{F}_{u,n} + \sum_{n=N/2+1}^N \varsigma_{l,n} \mathbf{F}_{l,n},$$

so that the boundary condition of (4) becomes

$$\left( \sum_{n=1}^{N/2} \varsigma_{u,n} L\mathbf{F}_{u,n} + \sum_{n=N/2+1}^N \varsigma_{l,n} L\mathbf{F}_{l,n} \right) = \mathbf{E}_{imp}^{\tan}$$

it is readily verified that generalized impedance matrix is then given by

$$[Z] = \begin{bmatrix} \langle \mathbf{W}_{u,1}, L\mathbf{F}_{u,1} \rangle & \dots & \langle \mathbf{W}_{u,1}, L\mathbf{F}_{u,N/2} \rangle \\ \langle \mathbf{W}_{u,2}, L\mathbf{F}_{u,1} \rangle & \dots & \langle \mathbf{W}_{u,2}, L\mathbf{F}_{u,N/2} \rangle \\ \dots & \dots & \dots \\ \langle \mathbf{W}_{u,N/2}, L\mathbf{F}_{u,1} \rangle & \dots & \langle \mathbf{W}_{u,N/2}, L\mathbf{F}_{u,N/2} \rangle \\ \dots & \dots & \dots \\ \langle \mathbf{W}_{l,N}, L\mathbf{F}_{u,1} \rangle & \dots & \langle \mathbf{W}_{l,N}, L\mathbf{F}_{u,N/2} \rangle \end{bmatrix} \quad (10)$$

$$\begin{bmatrix} \langle \mathbf{W}_{u,1}, \mathbf{LF}_{l, N/2+1} \rangle & \dots & \langle \mathbf{W}_{u,1}, \mathbf{LF}_{l, N} \rangle \\ \langle \mathbf{W}_{u,2}, \mathbf{LF}_{l, N/2+1} \rangle & \dots & \langle \mathbf{W}_{u,2}, \mathbf{LF}_{l, N} \rangle \\ \dots & \dots & \dots \\ \langle \mathbf{W}_{u, N/2}, \mathbf{LF}_{l, N/2+1} \rangle & \dots & \langle \mathbf{W}_{u, N/2}, \mathbf{LF}_{l, N} \rangle \\ \dots & \dots & \dots \\ \langle \mathbf{W}_{l, N}, \mathbf{LF}_{l, N/2+1} \rangle & \dots & \langle \mathbf{W}_{l, N}, \mathbf{LF}_{l, N} \rangle \end{bmatrix}.$$

A typical entry into the matrix of (10) is easily identified as

$$z_{s,m,t,n} = \int_{axis} dl \int_C dl' \left( j\omega\mu \mathbf{W}_{s,m} \cdot \mathbf{F}_{t,n} + \frac{1}{j\omega\epsilon} \frac{dW_{s,m}}{dl'} \frac{dF_{t,n}}{dl} \right) \frac{e^{-jkR_v}}{4\pi R_v}. \quad (11)$$

In (11), 's', 't', and 'v' can be either of 'u' (for the upper arm) or 'l' (for the lower arm), as may apply, to complete the formulation, (and hence the antenna's internal electrodynamic problem), the variable 'R' featuring in the Green's function in (11) requires specification. The respective position vectors for points on the upper arm on the wire surface and along the wire axis are given by

$$(\mathbf{r}; \mathbf{r}') = (l \cos \alpha \hat{\mathbf{a}}_y + l \sin \alpha \hat{\mathbf{a}}_z; l' \cos \alpha \hat{\mathbf{a}}_y + l' \sin \alpha \hat{\mathbf{a}}_z),$$

'R<sub>v</sub>' appearing in the equation is readily determined [21], as either

$$R_u = |\mathbf{r} - \mathbf{r}'| = \sqrt{b^2 + (l - l')^2},$$

in which 'b' represents the wire radius and which applies when the expansion function is specified on the upper arm; or for the lower arm, for which

$$(\mathbf{r}; \mathbf{r}') = (a(1 - \cos \psi) \hat{\mathbf{a}}_y - a \sin \psi \hat{\mathbf{a}}_z;$$

$$a(1 - \cos \psi') \hat{\mathbf{a}}_y - a \sin \psi' \hat{\mathbf{a}}_z), \text{ as}$$

$$R_l = \sqrt{b^2 + a^2 \left( 4 \sin^2 \left( \frac{\psi - \psi'}{2} \right) \right)},$$

in this case. Corresponding expressions for the other antenna structures in Fig. 1 share similarities with these results, as evident from the following considerations. In the case of the convex-Nu's lower arm,

$$(\mathbf{r}; \mathbf{r}') = (a \sin \psi \hat{\mathbf{a}}_y - a(1 - \cos \psi) \hat{\mathbf{a}}_z;$$

$$a \sin \psi' \hat{\mathbf{a}}_y - a(1 - \cos \psi') \hat{\mathbf{a}}_z)$$

and it is easy to see that  $R_l$  for this structure reduces to the same as that for the concave-Nu. Both structures share identical expressions for  $R_u$ , since up-

per arm geometry is the same in both cases. Position vectors of interest to the conventional Nu's upper and lower arms are given, respectively, by

$$(\mathbf{r}; \mathbf{r}') = (a \sin \psi \hat{\mathbf{a}}_y + a(1 - \cos \psi) \hat{\mathbf{a}}_z;$$

$$a \sin \psi' \hat{\mathbf{a}}_y + a(1 - \cos \psi') \hat{\mathbf{a}}_z) \text{ and}$$

$$(\mathbf{r}; \mathbf{r}') = (a(1 - \cos \psi) \hat{\mathbf{a}}_y - a \sin \psi \hat{\mathbf{a}}_z;$$

$$a(1 - \cos \psi') \hat{\mathbf{a}}_y - a \sin \psi' \hat{\mathbf{a}}_z).$$

From which it follows that for this curvilinear structure,

$$R_l = R_u = \sqrt{b^2 + a^2 \left( 4 \sin^2 \left( \frac{\psi - \psi'}{2} \right) \right)}.$$

Finally, it is not difficult, for the V-dipole, to verify that

$$R_u = R_l = \sqrt{b^2 - (l - l')^2}.$$

The next step in the analysis is the formulation of the external electrodynamic problem, which is that of determining the radiation zone fields. In the far-zone, the electric field intensity is related to the vector magnetic potential according to  $\mathbf{E}(\mathbf{r}) = -j\omega \mathbf{A}(\mathbf{r})$ ,  $r \gg r'$ .  $\mathbf{A}$  is still prescribed by (2a) but unlike the  $\mathbf{A}$  for the internal problem, it is given, for example, in the case of the concave dipole's upper arm, by

$$\mathbf{A}_u = \frac{\mu e^{-jkr}}{4\pi r} \int_0^{L_u} (\cos \alpha \hat{\mathbf{a}}_y + \sin \alpha \hat{\mathbf{a}}_z) \times \\ \times I(\ell') e^{jk\ell' [\sin \theta \sin \phi \cos \alpha + \cos \theta \sin \alpha]} d\ell',$$

in which, for the Green's function, use has been made of

$$R = |\mathbf{r} - \mathbf{r}'| \approx \begin{cases} r - \mathbf{r} \cdot \mathbf{r}', & \text{phase approximation;} \\ r, & \text{magnitude approximation} \end{cases}$$

with

$$\mathbf{r}' = l' \cos \alpha \hat{\mathbf{a}}_y + l' \sin \alpha \hat{\mathbf{a}}_z.$$

Accordingly, and using the well-known Cartesian to spherical coordinates transformation identity, the spherical coordinates components of the contributions of this arm to the structure's radiation zone field emerge as

$$E_{\theta u} = \frac{-j\omega\mu e^{-jkr}}{4\pi r} \int_0^{L_u} [\cos \theta \sin \phi \cos \alpha - \sin \theta \sin \alpha] \times \quad (12)$$

$$\times I(\ell') e^{jk\ell' [\sin \theta \sin \phi \cos \alpha + \cos \theta \sin \alpha]} d\ell',$$

$$E_{\phi u} = \frac{-j\omega\mu e^{-jkr}}{4\pi r} \int_0^{L_u} \cos \phi \cos \alpha I(\ell') \times$$

$$\times e^{jk\ell' [\sin \theta \sin \phi \cos \alpha + \cos \theta \sin \alpha]} d\ell'.$$



Following similar steps, it is fairly straightforward to establish that corresponding expressions for the structure's lower arm is

$$\begin{aligned} E_{\theta l} = & \quad (13) \\ = & \frac{-j\omega\mu e^{-jkr}}{4\pi r} \int_0^{\pi/2} [\cos\theta \sin\varphi \sin\psi' + \sin\theta \cos\psi'] \times \\ & \times I(\psi') e^{jka[\sin\theta \sin\varphi(1-\cos\psi') - \cos\theta \sin\psi']} d\psi', \\ E_{\phi l} = & \frac{-j\omega\mu e^{-jkr}}{4\pi r} \int_0^{\pi/2} [\cos\varphi \sin\psi'] \times \\ & \times I(\psi') e^{jka[\sin\theta \sin\varphi(1-\cos\psi') - \cos\theta \sin\psi']} d\psi'. \end{aligned}$$

According to (12) and (13), the theta-component of this field vanishes in the antenna's YZ plane, where  $\varphi = 90^\circ$ . Therefore, the concave-Nu dipole's radiation field as given in that plane, by the superposition of (12) and (13), is obtained as

$$\begin{aligned} E_{\theta cnv} = & \frac{-j\omega\mu e^{-jkr}}{4\pi r} \left( \int_0^{L_u} [\cos(\theta + \alpha)] \times \right. \\ & \times I(\ell') e^{jk\ell' \sin(\theta + \alpha)} d\ell' + \\ & + \int_0^{\pi/2} a \sin(\theta + \psi') I(\psi') \times \\ & \times e^{jka[\sin\theta \sin\varphi(1-\cos\psi') - \cos\theta \sin\psi']} d\psi' \Big). \end{aligned} \quad (14)$$

Using the same reasoning, radiation-zone fields in the YZ plane for the other three curvilinear structures are readily determined as

$$\begin{aligned} E_{\theta cvx} = & \frac{-j\omega\mu e^{-jkr}}{4\pi r} \left( \int_0^{L_u} [\cos(\theta + \alpha)] \times \right. \\ & \times I(\ell') e^{jk\ell' \sin(\theta + \alpha)} d\ell' + \\ & + \int_0^{\pi/2} a \sin(\theta + \psi') I(\psi') \times \\ & \times e^{jka[\sin\theta \sin\varphi(1-\cos\psi') - \cos\theta \sin\psi']} d\psi' \Big) \end{aligned} \quad (15)$$

for the convex-Nu dipole;

$$\begin{aligned} E_{\theta cvnu} = & \frac{-j\omega\mu a e^{-jkr}}{4\pi r} \times \\ = & \left[ \int_0^{\pi/2} \left( \cos(\theta + \psi') I(\psi') e^{jka[\cos(\theta + \psi') + \cos\theta]} + \right. \right. \end{aligned} \quad (16)$$

$$\begin{aligned} & + a \sin(\theta + \psi') I(\psi') \times \\ & \times e^{jka[\sin\theta \sin\varphi(1-\cos\psi') - \cos\theta \sin\psi']} \Big) d\psi' \Big] \end{aligned}$$

for the convex-Nu; and finally,

$$\begin{aligned} E_{\theta vda} = & \frac{-j\omega\mu e^{-jkr}}{4\pi r} \times \\ & \times \left( \int_0^{L_u} [\cos(\theta + \alpha)] I(\ell') e^{jk\ell' \sin(\theta + \alpha)} d\ell' + \right. \\ & + \left. \left( \int_0^{L_l} [\cos(\theta - \alpha)] I(\ell') e^{jk\ell' \sin(\theta - \alpha)} d\ell' \right) \right). \end{aligned} \quad (17)$$

for the Vee-dipole antenna.

Once the desired current distributions become available through the method of moments, therefore, it becomes a fairly straightforward matter to determine antenna performance parameters of interest. For this paper, these parameters, in addition to far-zone patterns, include feed point input admittance given by

$$Y_{in} = \frac{I_{in}}{V_{in}} = G_{in} + jB_{in},$$

where  $G_{in}$  stands for input conductance and  $B_{in}$  input susceptance. Others are return loss, which, as pointed out by [23], is defined as

$$Return\ Loss(dB) = 20 \log_{10} \left| \frac{Z_{in} + Z_o}{Z_{in} - Z_o} \right|,$$

where, in this paper,  $Z_o = 50\Omega$  and  $Z_{in} = 1/Y_{in}$  represents the feed point input impedance of the curvilinear configuration of interest. Finally, maximum directivity, a common performance assessment metric for curvilinear antenna structures, [1–5], is determined using the well-known expression, [24];

$$D_{max} = 10 \log_{10} \left( \frac{4\pi U_{max}}{P_{rad}} \right) (dB),$$

in which  $U_{max}$  represents maximum radiation intensity and  $P_{rad}$ , the total radiated power; both evaluated using the following respective equations:

$$U_{max} = \left( \frac{1}{2\eta} \left[ |E_{\theta}(\theta, \varphi)|^2 + |E_{\phi}(\theta, \varphi)|^2 \right] \right)_{max},$$

and

$$P_{rad} = \int_{\varphi=0}^{2\pi} \int_{\theta=0}^{\pi} U \sin\theta d\theta d\varphi.$$

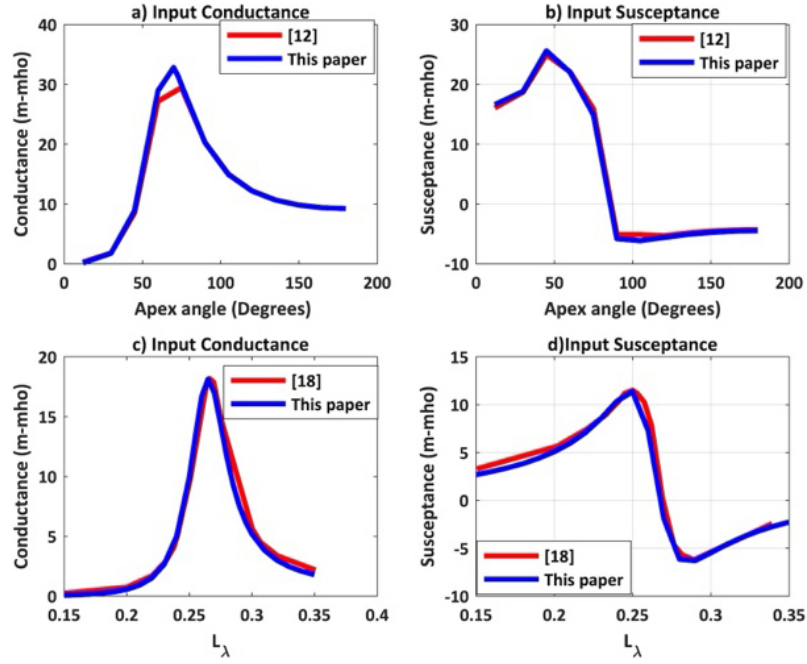


Fig. 3. Comparison of input admittance profiles published in [12] and [18] with corresponding results of this paper

Рис. 3. Сравнение профилей входной проводимости, опубликованных в [12] и [18], с соответствующими результатами настоящей статьи

## 2. Computational results and discussion

For all the computational results presented and discussed in this section, a delta-gap feed model with an excitation voltage of 1 V was utilized. In addition, for the center frequency of 1,5 GHz, the thin-wire property of all the structures are maintained through meeting the requirement that  $0,002\lambda \leq \text{wire radius} \leq 0,008\lambda$ . Piece-wise linear functions are utilized as both expansion and weighting functions, in a Galerkin's approach, whose details (including approximations, convergence properties, and error bounds) are comprehensively described in [20–22].

As a check on the validity of the paper's analytical formulation of section 1 concerning the internal problem, input admittance results published in [12] and [18] are compared with corresponding results obtained with the use of this paper's formulation. Outcomes of the comparisons are displayed in Fig. 3.

The profiles of Fig. 3, *a, b* compare the input admittance data of the VDA with dimensions given in Table 2 of [12], with computational results for the same VDA, obtained with this paper's formulation. Also, the input admittance comparisons of Fig. 3, *c, d*, are for the concave Nu dipole treated in [18, Fig. 2] and corresponding computational data due to this paper. The very close agreements between these profiles lend credence to the validity of the formulation in this paper.

Current distribution characteristics are compared for the four configurations, by the profiles of Fig. 4 (magnitude) and Fig. 5 (phase).

From the curves displayed in first row of Fig. 4, it can be seen that when the half-arm length is limited to  $0,25\lambda$  for all the curvilinear structures, magnitude of current varies significantly with apex angle  $\alpha$ . When  $\alpha$  changes from  $30^\circ$  to  $50,4^\circ$ , for example, magnitude of current for the V-dipole became generally halved in size. Furthermore magnitude of current for the convex-Nu dipole increased significantly, generally becoming larger than corresponding values for the V-dipole. At  $\alpha = 60^\circ$ , values of magnitude of current recorded for the convex-Nu drastically reduced from those recorded at  $\alpha = 50,4^\circ$ . Profiles of magnitude of current displayed in Fig. 5, *d, e, f*, for the  $L = 0,75\lambda$  cases are generally comparable for all the curvilinear configurations, for  $\alpha = 50,4^\circ$ . For the other two values of apex angle, values recorded for the concave-Nu and convex-Nu structures are noticeably smaller.

The phase distribution curves of Fig. 5, *a, b, c*, (for  $L = 0,25\lambda$  cases) underscore a property implicitly stated in [3] that shaping the dipole represents a method of prescribing a phase distribution for the wire antenna. It can be seen from Fig. 5, *a*, for example, values recorded for V-dipole are positive, whereas, corresponding values recorded the convex-Nu and concave -Nu structures (with one arm shaped and the other linear), are negative. On the other hand, as can be seen from Fig. 5, *b*, values recorded

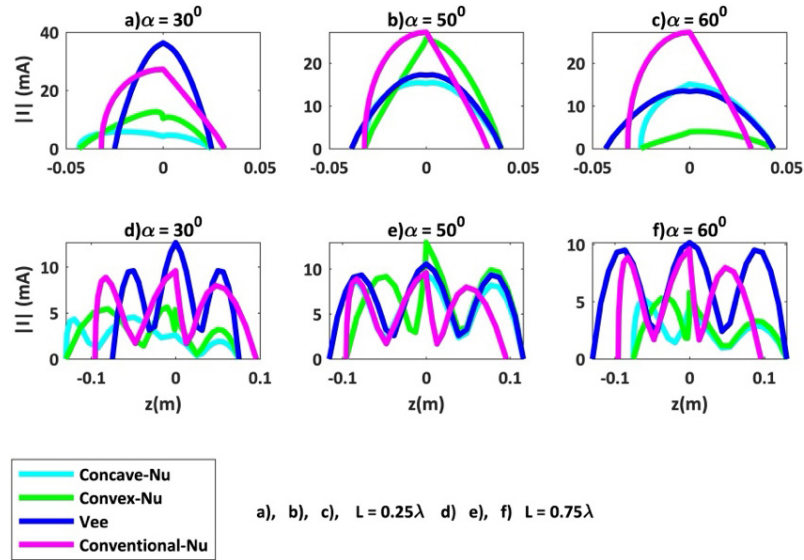


Fig. 4. Profiles of distribution of magnitude of current for the curvilinear antennas for various apex angles  
Рис. 4. Профили распределения величины тока для криволинейных антенн при различных углах при вершине

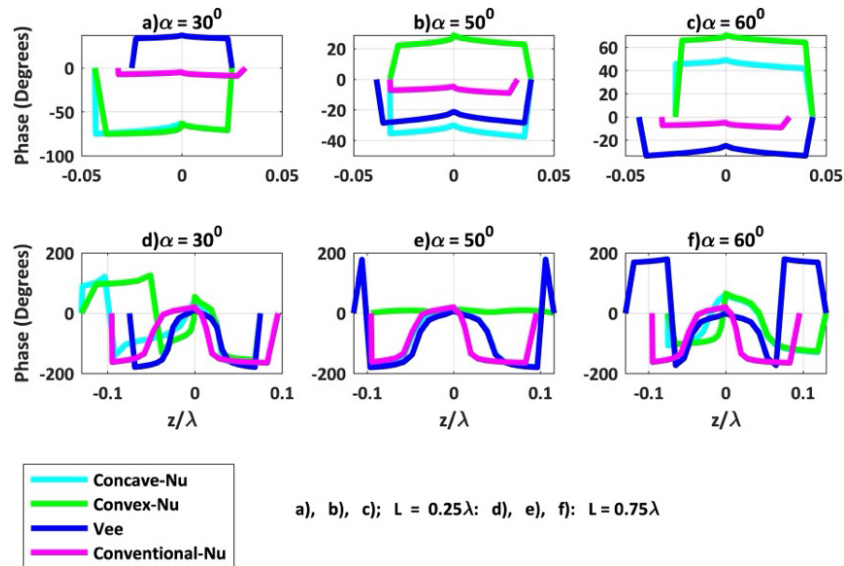


Fig. 5. Phase distribution profiles corresponding to the magnitude profiles of Fig. 4  
Рис. 5. Профили распределения фаз, соответствующие профилям магнитуд рис. 4

for the V- and Convex-Nu – dipoles reversed in sign from corresponding values displayed in Fig. 5, *a*, indicating that for  $L = 0,25\lambda$  curvilinear dipole, apex angle represents another parameter choice for prescribing phase distribution of axially directed current flow. It should be pointed out that all the curves in both Fig. 4 and 5 for the conventional-Nu configuration, are independent of apex angle, as the geometry is only related to the others, through choice of half arm length,  $L$ . Finally, the curves of Fig. 5, *d, e, f*, describe corresponding phase distributions for all four configurations, when half arm length is fixed at  $0,75\lambda$ . The phase reversals occurring here are cases are not as pronounced as those earlier described for the  $L = 0,25\lambda$  cases. With the exception of the curves

for the convex-Nu structure, such phase reversals as are recorded, are essentially limited to segments close the ends of the arms of the antenna.

## 2.1. Influence of slant angle on the performance of the Nu dipole

As observed in [9; 25], the introduction of geometrical asymmetry in the curvilinear dipole antenna's structure has significant effects on the antenna's performance. This influence is not well-captured in the treatment of the concave Nu dipole presented in [18], mainly because only one value of slant angle ( $\alpha = 60^\circ$ ) was considered in that publication. A relationship between relative arms' lengths and slant angle may be conveniently established by



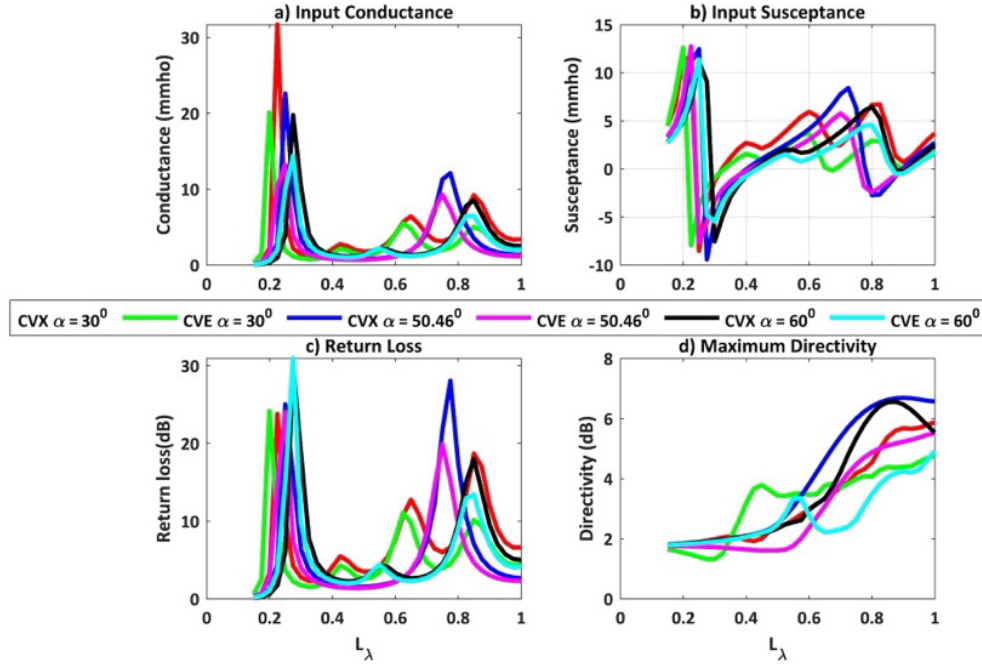


Fig. 6. Profiles of input admittance, return loss and maximum directivity for different values of slant angle

Рис. 6. Профили входной проводимости, обратных потерь и максимальной направленности для различных значений угла наклона

projecting both arms on the y-axis. The projection of the upper arm (of length  $L_u$ ) of the concave Nu dipole on the y-axis is  $L_u \cos \alpha$ . When it is noted that the lower arm is a quarter of a circle (of radius  $a$ ) in extent, and letting  $L_l$  represent the physical length of this arm, it becomes easy to see that  $a = 2L_l / \pi$ . Hence, both arms will have equal projections on the y-axis, when

$$L_u \cos \alpha = \frac{2L_l}{\pi}, \quad (18)$$

so that the desired relationship between the arms' lengths emerges as

$$L_u = \frac{2}{\pi \cos \alpha} L_l. \quad (19)$$

For a given radius of the arc representing the lower arm, therefore, the relative lengths of both arms are determined by slant angle according to (12)–(13) as

$$\alpha = \cos^{-1} \left( \frac{2 L_l}{\pi L_u} \right). \quad (20)$$

Three possible scenarios, namely, the cases of  $L_u < L_l$ ,  $L_u = L_l$ , and  $L_u > L_l$ , are of particular interest; and it is readily verified that the choices of  $\alpha = 30^\circ$  ( $L_u = 0.75L_l$ ),  $\alpha = 50.46^\circ$  ( $L_u = L_l$ ), and  $\alpha = 60^\circ$  ( $L_u = 1.25L_l$ ), respectively, define the geometries of the three scenarios.

With reference to these three values of slant angle, an illustration of the effects of differences in arms' lengths extent for both the convex- and concave -Nu dipole antennas is provided by the profiles of Fig. 6.

Here, (and elsewhere in this paper),  $L_\lambda = L_u / \lambda$ , and the associated  $L_l$ , for any given  $\alpha$ , is specified by (13)–(14)

The profiles of Fig. 6, a, for input conductance ( $G_{in}$ ), display two sets of maxima for  $G_{in}$ ; the first set, located in the region  $0.2 < L_\lambda < 0.4$ , and the second,  $0.6 < L_\lambda < 0.9$ . For the first set of maxima, the largest values were recorded by the convex-Nu dipole with slant angles of  $30^\circ$ ,  $50.46^\circ$ , and  $60^\circ$ , in that order.

The order of occurrence of  $G_{in}$  maxima differs slightly for the concave-Nu dipole in that the  $60^\circ$  maximum occurs before that of  $50.46^\circ$ . Maxima recorded by the convex-Nu dipole in the second set are also generally higher than those recorded by the concave-Nu configuration; though in the latter case, the largest value was recorded by the  $50.46^\circ$  convex-Nu configuration. A notable feature of the  $B_{in}$  profiles of Fig. 6, b, is that for  $L_u < L_l$  ( $\alpha = 30^\circ$ ), the convex-Nu dipole resonates only at two values of  $L_\lambda$  (0.22 and 0.25), whilst the other four, each resonate for four different values of  $L_\lambda$ . It is also noteworthy that for this latter case, two sets of resonant lengths are in close proximity; one in the neighborhood of  $L_\lambda = 0.45$ , and the other, in the vicinity of  $L_\lambda = 0.90$ .

Variations of return loss with arms' lengths for different values of apex angle, are displayed in Fig. 6, c. The profiles clearly fall into the two categories earlier described for  $G_{in}$ . Return loss for the first set reveal that maxima, of the  $\alpha = 60^\circ$  configurations had the largest values (with that for the concave-Nu slightly

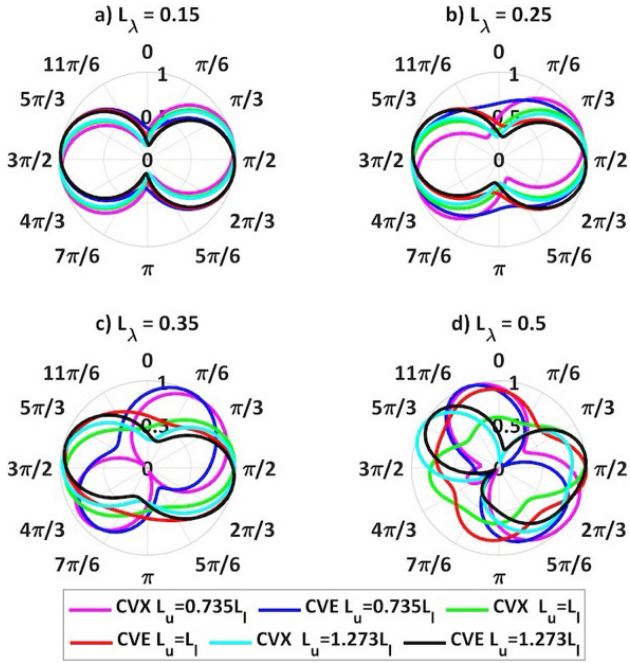


Fig. 7. Comparison of radiation-zone field patterns for the three convex-Nu and concave-Nu configurations with  $0.15 \leq L_\lambda \leq 0.50$   
Рис. 7. Сравнение диаграмм направленности для трех конфигураций выпуклого Nu и вогнутого Nu при  $0.15 \leq L_\lambda \leq 0.50$

greater), whereas, values recorded by the other four configurations featured marginal differences. For the second set, the  $\alpha = 50.46^\circ$  convex-Nu and  $\alpha = 30^\circ$  concave-Nu configurations recorded the distinctly largest and least values of return loss, respectively. Finally, it can be seen from the maximum directivity profiles of Fig. 6, d, that values for the convex-Nu configurations are significantly larger than those of the concave-Nu configurations.

The largest maximum directivity values (close to 7 dB) are those for the  $50.46^\circ$  and  $60^\circ$  convex-Nu configurations, in that order.

A number of interesting features are revealed by the far-field patterns in the antenna plane, displayed in Fig. 7. For normalized upper length arm ( $L_\lambda$ ) of 0.15, the field pattern profiles of Fig. 7, a, share similar shapes (referred to in [24] as ‘azimuth’, and similar to Fig. 2 of [18]) for all values of slant angle. From Fig. 7, b, for  $L_\lambda = 0.25$ , it can be seen that the symmetry displayed in Fig. 7, a, no longer features in all cases. As a matter of fact, in this case, the pattern due to the concave-Nu with  $\alpha = 30^\circ$  assumes a form that may be described as ‘quasi-omnidirectional’. In addition to the ‘rotation of orientation’ described in [18], the patterns of Fig. 7, c, include another ‘quasi-omnidirectional’ pattern, this time, due to the convex-Nu with  $\alpha = 30^\circ$  configuration.

The pattern shape deformation, which may be said to have initiated in Fig. 7, d, manifests as minor lobes

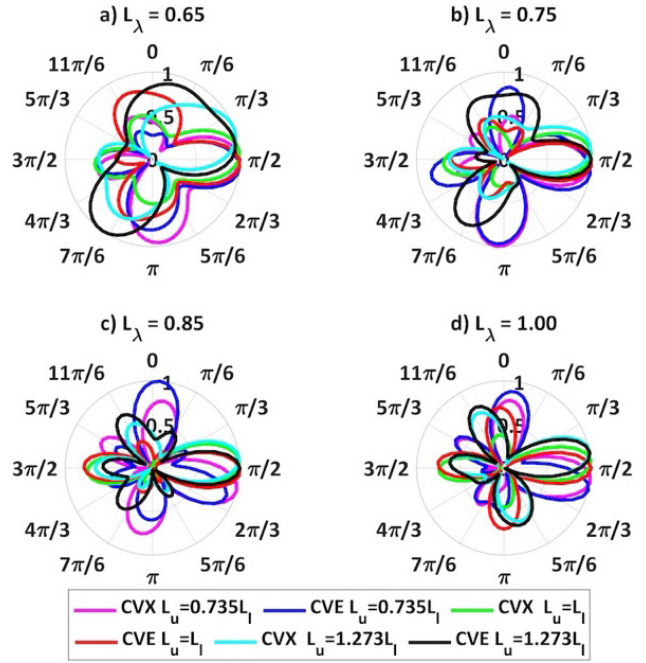


Fig. 8. Comparison of radiation-zone field patterns for the three convex-Nu and concave-Nu configurations with  $0.65 \leq L_\lambda \leq 1.00$   
Рис. 8. Сравнение картин поля зоны излучения для трех конфигураций выпуклого Nu и вогнутого Nu при  $0.65 \leq L_\lambda \leq 1.00$

in the field patterns of Fig. 8, a–d. From the profiles of Fig. 8, a, it is easy to see that in terms of sharpness of main lobe and corresponding minor lobe sizes, the best performing configuration is the  $50.46^\circ$  convex-Nu, followed by the  $30^\circ$  convex-Nu, with the  $60^\circ$  concave performing worst here, and indeed, in all other cases. Profiles of Fig. 8, b, follow the same general trend, but there are two notable exceptions: first, the second best performing configuration in this case, is the  $60^\circ$  convex-Nu; and second, the  $50.46^\circ$  concave-Nu now performs better than the  $30^\circ$  concave-Nu. For  $L_\lambda = 1.00$ , the convex-Nu configurations ( $50.46^\circ$ ,  $60^\circ$  and  $30^\circ$ , in that order) are collectively and individually better performing than the corresponding concave-Nu configurations.

## 2.2. Comparison of concave-Nu, Convex-Nu, Conventional-Nu and conventional V configurations

Discussions in the preceding section (2.1) established that the convex-Nu curvilinear configuration of the VDA represents a better performing configuration than its concave-Nu counterpart.

In this section, the performances of both configurations are compared with those of the conventional-Nu and conventional V dipole antennas. Candidates for the comparisons include the representative  $50.46^\circ$  convex- and concave-Nu configurations, the symmetrical VDA with an apex angle of  $50.46^\circ$ , and arms lengths equal to  $L_u$  of the Nu dipoles; as well as

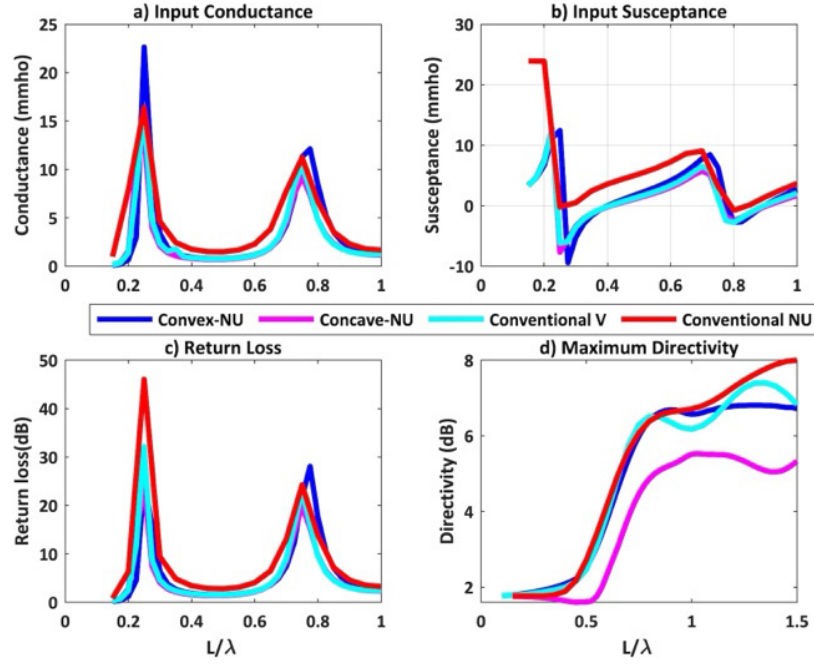


Fig. 9. Comparison of input admittance, return loss and maximum directivity profiles

Рис. 9. Сравнение профилей входной проводимости, обратных потерь и максимальной направленности

the conventional-Nu. From the first set of  $G_{in}$  maxima of the profiles of Fig. 9, a, it can be seen that the values recorded by the conventional-Nu and VDA, in that order, are larger than those for the convex- and concave-Nu configurations.

The second set differs only in that the convex-Nu now recorded the largest value of  $G_{in}$ . According to the  $B_{in}$  profiles of Fig. 7, b, the VDA and convex- / concave-Nu configurations all share two resonance lengths; one close to  $L = 0,4\lambda$ , and the other, in the vicinity of  $L = 0,9\lambda$ . The conventional- and convex-Nu configurations also share the two resonance lengths of about  $0,25\lambda$  and  $L = 0,76\lambda$ .

A particularly noteworthy feature of the return loss profiles of Fig. 9, c, is the remarkably large value (close to 50 dB) for the conventional-Nu configuration. It may also be noted that maximum return loss for the VDA is larger than that for the convex-Nu, which in turn, and as noted in section 3.1, is larger than that for the concave-Nu. With the exception of the concave-Nu configuration, (whose maximum directivity is distinctly the least over virtually the entire spectrum of  $L_\lambda$  considered in this paper) maximum directivity values are comparable for values of  $L_\lambda$  up to about 0,75. Beyond this point, maximum directivity for the convex-Nu 'saturates' to a value of about 6,25 dB, that for the VDA rises to a value of about 7 dB (at  $L_\lambda = 1,25$  dB) before falling to the 'saturation' value for the convex-Nu; whilst that for the conventional-Nu rises steadily to 8,01 dB at  $L = 1,5\lambda$ . Two

important conclusions are indicated by these results; the first is that the conventional-Nu dipole is capable of achieving a maximum directivity greater than the 7 dB reported [6] for the  $3\lambda/2$  optimum shape (Gauss) wire dipole: and second, that as suggested by [24], a  $5\lambda/2$  shaped (curvilinear) configuration is also capable of achieving improved directivity metrics.

Radiation-zone field patterns for the four configurations are compared in Fig. 10 for 'upper arm' length in the range  $0,75 \leq L_\lambda \leq 1,50$ , over which maximum directivity is distinct. In Fig. 10, a, the pattern for the conventional-Nu has its main lobe directed along the  $130-310^\circ$  axis, whereas those for the other three are more or less, all directed along the  $90-270^\circ$  axis. The patterns of Fig. 10, b, are also multi-lobed like those of the others, but in this case, the minor lobes are more uniformly shaped, on account of the nulls that now feature in all the patterns. Although the orientations of the main lobes remain as earlier described for the patterns of Fig. 10, a, the main beams are generally sharper, suggesting that the associated maximum directivity profiles are mainly due to minor lobe sizes. Beyond  $L_\lambda = 1,0$ , the nulls that featured in the patterns of Fig. 8, b, vanish, as evident from Fig. 10, c-d; the main beams are sharper though, with those for the conventional-Nu approaching the 'pencil-beam' variety.

An alternative view of the field patterns of Fig. 10 is presented in Fig. 11, where, for each configuration, profiles of the radiation-zone patterns are compared,

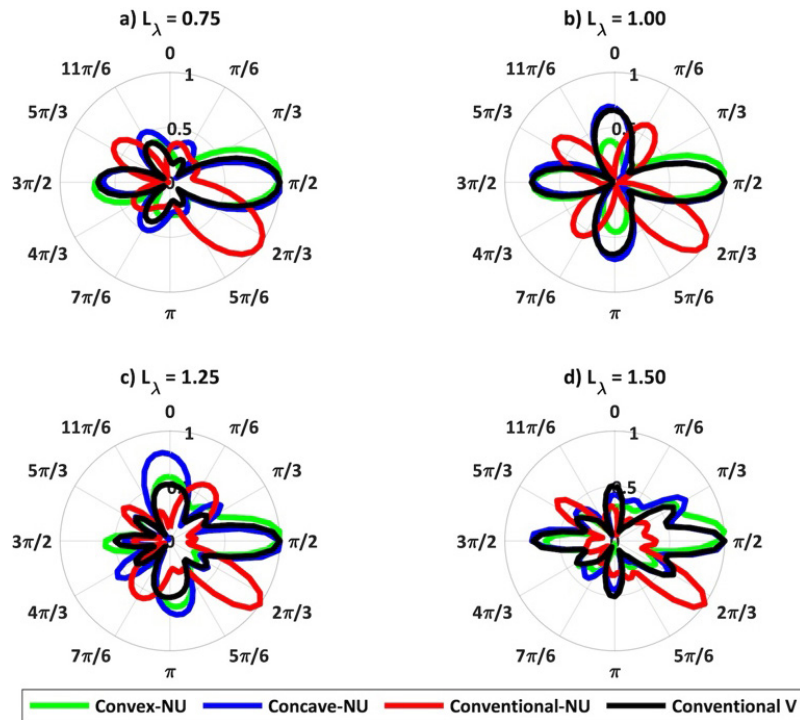


Fig. 10. Comparison of profiles of far-zone field patterns  
Рис. 10. Сравнение профилей поля дальней зоны

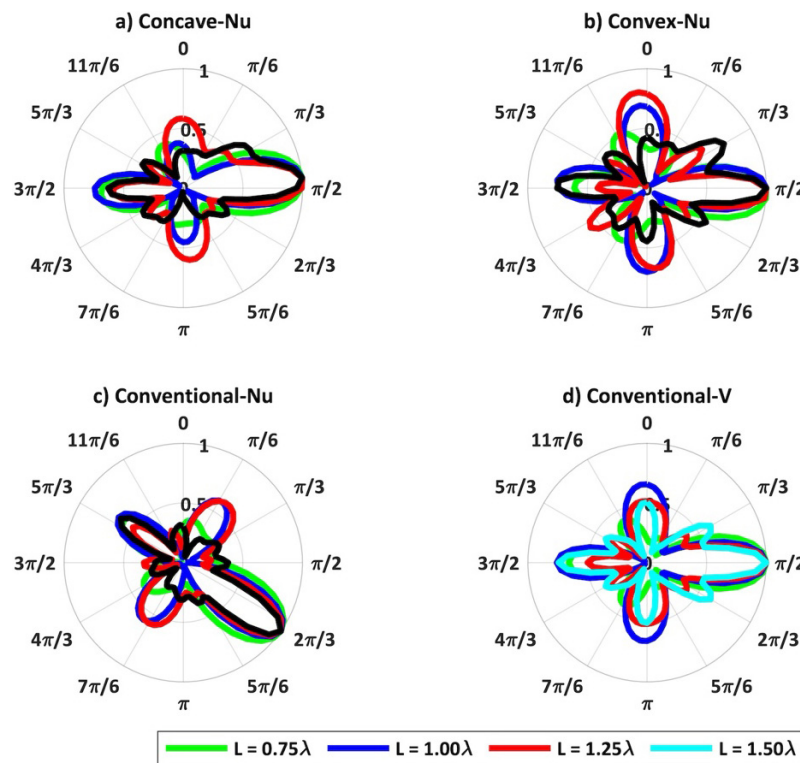


Fig. 11. An alternative view of the far-zone patterns of Fig. 10  
Рис. 11. Альтернативный вид полей дальней зоны рис. 10

for varying values of  $L_\lambda$ . Because the responses of the convex-NU and concave-NU configurations in this connection have earlier been discussed, only those for the conventional-NU and conventional-V need be described. Thus, and with reference to Fig. 11, c, the

pattern for the  $L_\lambda = 1,50$  conventional-NU case has the sharpest main lobe, followed by  $L_\lambda = 1,25, 1,00$  and  $0,75$ , in that order. Minor lobes contributions to corresponding patterns' average intensities, however, are generally in the reverse order. The same trend is



followed by the profiles displayed in Fig. 11, *d*, for the conventional V dipole, whose far-zone patterns exhibit slightly poorer directivity properties than those of corresponding conventional-Nu dipole antennas.

## Conclusion

A comprehensive comparative performance analysis of three curvilinear configurations (here referred to as the concave-Nu, convex-Nu, and conventional-Nu) of the V-dipole antenna has been presented in this paper. Integral field expressions rigorously formulated for each of the configurations had the distribution of current along the axis of the antenna as the only unknown. The unknown current distributions were determined through the use of the method of moments, following which computational results for input conductance, return loss, maximum directivity, and far-zone radiation fields in the antenna plane, became available.

First, the computational results established that for the convex-Nu/concave-Nu configurations, choice of length of linear arm and its slant angle,  $\alpha$ , (which also prescribes degree of curvature of curved arm) significantly influenced antenna response. And following a comparison of the aforementioned performance metrics, it was established for the first

time, that the convex-nu configuration represents a much better performing configuration than the concave-Nu introduced by [18]. When the performances of these two configurations were compared with those of the conventional-Nu and conventional-V configurations, the metrics revealed that the best performing of the lot is the conventional-Nu configuration, particularly with reference to return loss and maximum achievable directivity. Indeed, the 8 dB maximum directivity recorded for the conventional-Nu configuration is significantly better than the 7,13 dB reported for the optimum-shaped wire (Gauss) dipole in [6]. It is also noteworthy that the return loss of close to 50 dB recorded by the conventional-Nu dipole antenna is by far better than those recorded by the other three configurations.

A number of possibilities for future investigations are offered by the analysis presented in this paper. One of such possibilities concerns the influence of asymmetry of the type described in [9], on the performance of the conventional-Nu configurations. Others are the possibility of the configuration's directivity performance enhancement through the introduction of a small ground plane into its structure: and that of resistively loading the configuration towards deployment in ground penetrating radar (GRR) applications, as common with conventional-V dipoles.

## References

1. F. Landstorfer, "A new type of directional antenna," 1976 *Antennas and Propagation Society International Symposium*, pp. 169–172, 1976, doi: <https://doi.org/10.1109/APS.1976.1147636>.
2. F. M. Landstorfer, "New developments in VHF/UHF antennas," *International Conference on Antennas and Propagation. Proceedings*, part 1, pp. 132–141, 1978.
3. J. Kataja and K. Nikoskinen, "The parametric optimization of wire dipole antennas," *IEEE Transactions on Antennas and Propagation*, vol. 59, no. 2, pp. 350–356, 2011, doi: <https://doi.org/10.1109/TAP.2010.2096181>.
4. W. Junhong and R. Lang, "Directivity optimization of curved surface dipole antennas," *Journal of Electronics (China)*, vol. 11, no. 4, pp. 322–331, 1994, doi: <https://doi.org/10.1007/BF02778386>.
5. W. Jun-Hong and J. Lang, "Analysis of curvilinear dipoles and their arrays with finite reflectors," *Proceedings of IEEE Antennas and Propagation Society International Symposium and URSI National Radio Science Meeting*, vol. 2, pp. 1002–1006, 1994, doi: <https://doi.org/10.1109/APS.1994.407919>.
6. D. K. Cheng and C. H. Liang, "Shaped wire antennas with maximum directivity," *Electronics Letters*, vol. 18, no. 19, pp. 816–818, 1982, doi: <https://doi.org/10.1049/el:19820555>.
7. C. H. Liang and D. K. Cheng, "Directivity optimization for Yagi-Uda arrays of shaped dipoles," *IEEE Transactions on Antennas and Propagation*, vol. 31, no. 3, pp. 522–525, 1983, doi: <https://doi.org/10.1109/TAP.1983.1143085>.
8. W. Chen, L. Jen, and S. M. Zhang, "Radiation pattern optimisation for Yagi-Uda arrays of shaped dipole antennas," *Electronics Letters*, vol. 30, no. 16, pp. 1264–1265, 1994, doi: <https://doi.org/10.1049/el:19940877>.
9. Z. Cai et al., "Optimization of shaped wire antennas for asymmetric excitation," *International Conference on Microwaves and Communications (ICMC)*, pp. 316–319, 1992, url: <https://www.ece.uvic.ca/~jbornema/Conferences/023-92icmc-cjbl.pdf>.
10. C. Tang, "Input impedance of arc antennas and short helical radiators," *IEEE Transactions on Antennas and Propagation*, vol. 12, no. 1, pp. 2–9, 1964, doi: <https://doi.org/10.1109/TAP.1964.1138164>.
11. U. U. R. Qureshi et al., "Miniaturized arc shaped near isotropic self-complementary antenna for spectrum sensing applications," *Sensors*, vol. 23, no. 2, pp. 927, 2023. DOI: <https://doi.org/10.3390/s23020927>
12. D. M. Petković and D. D. Krstić, "A new approach to V-dipole antenna," *Facta Universitatis. Series: Working and Living Environmental Protection*, vol. 2, no. 2, pp. 143–149, 2002, url: <http://facta.junis.ni.ac.rs/walep/walep2002/walep2002-06.pdf>.



13. R. Blanchard et al., "Modeling nanoscale V-shaped antennas for the design of optical phased arrays," *Phys. Rev. B*, vol. 85, no. 15, pp. 155457-1-11, 2012, doi: <https://doi.org/10.1103/PhysRevB.85.155457>.
14. K. Kim and W. R. Scott, "Design of a resistively loaded vee dipole for ultrawide-band ground-penetrating radar applications," *IEEE Transactions on Antennas and Propagation*, vol. 53, no. 8, pp. 2525-2532, 2005, doi: <https://doi.org/10.1109/TAP.2005.852292>.
15. A. Mohamed and L. Shafai, "Investigation on vee dipole antennas for ultra-wideband applications," *2009 13th International Symposium on Antenna Technology and Applied Electromagnetics and the Canadian Radio Science Meeting*, pp. 1-4, 2009, doi: <https://doi.org/10.1109/ANTEMURSI.2009.4805093>.
16. J. H. Wang, L. Jen, and S. S. Jian, "Optimization of the dipole shapes for maximum peak values of the radiating pulse," *IEEE Antennas and Propagation Society International Symposium*, vol. 1, pp. 526-529, 1997, doi: <https://doi.org/10.1109/APS.1997.630214>.
17. I. Misra, R. Chakrabarty, and B. Mangaraj, "Design, analysis and optimization of V-dipole and its three-element Yagi-Uda array," *Progress in Electromagnetics Research*, vol. 66, pp. 137-156, 2006, doi: <https://doi.org/10.2528/PIER06102604>.
18. O. U. Okereke, "Analysis of Nu-dipole antenna using the method of moments," *International Journal of Electronics*, vol. 86, no. 12, pp. 1481-1492, 1999, doi: <https://doi.org/10.1080/002072199132563>.
19. D. P. Tabakov and B. M. Al-Nozaili, "Solving an internal problem for finite regular two-dimensional lattice spiral elements, excitable plate electromagnetic wave," *Physics of Wave Processes and Radio Systems*, vol. 27, no. 3, pp. 17-33, 2024, doi: <https://doi.org/10.18469/1810-3189.2024.27.3.17-33>. (In Russ.)
20. T. K. Sarkar, A. R. Djordjevic, and B. M. Kolundzija, "Method of moments applied to antennas," url: <https://mtt.etf.bg.ac.rs/Mikrotalasna.Tehnika/Clanci/ANTMOM.pdf>.
21. R. F. Harrington, "Matrix methods for field problems," *Proceedings of the IEEE*, vol. 55, no. 2, pp. 136-149, 1967, doi: <https://doi.org/10.1109/PROC.1967.5433>.
22. D. C. Kuo and B. J. Strait, "Improved programs for analysis of radiation and scattering by configuration of arbitrarily bent wires," *Syracuse University Scientific Report No. 15*, 1972, url: <http://ece-research.unm.edu/summa/notes/In/0275.pdf>.
23. T. S. Bird, "Definition and misuse of return loss [Report of the transactions editor-in-chief]," *IEEE Antennas and Propagation Magazine*, vol. 51, no. 2, pp. 166-167, 2009, doi: <https://doi.org/10.1109/MAP.2009.5162049>.
24. C. A. Balanis, *Antenna Theory: Analysis and Design*. New Jersey: John Wiley & Sons, Inc., 1997.
25. R. A. Burberry, *VHF and UHF Antennas*. London: Peter Peregrinus Ltd., 1992.

## Information about the Authors

**Ayotunde A. Ayorinde**, Ph.D. Electrical Engineering, senior lecturer, Department of Electrical and Electronics Engineering, University of Lagos, Akoka, Lagos, Nigeria.

*Research interests:* electromagnetics, antennas, radiowave propagation, computational methods.

*E-mail:* [aayorinde@unilag.edu.ng](mailto:aayorinde@unilag.edu.ng)

*ORCID:* <https://orcid.org/0009-0005-9731-8924>

**Sulaiman A. Adekola**, Ph.D. Electrical Engineering, emeritus professor, Department of Electrical and Electronics Engineering, University of Lagos, Akoka, Lagos, Nigeria.

*Research interests:* electromagnetics, antennas, radiowave propagation, acoustic (echosonde) antennas, RF energy harvesting.

*E-mail:* [adekolaadeniyi43@gmail.com](mailto:adekolaadeniyi43@gmail.com)

*ORCID:* <https://orcid.org/0000-0002-3926-5378>

**Ike Mowete**, Ph.D. Electrical Engineering, professor, Department of Electrical and Electronics Engineering, University of Lagos, Akoka, Lagos, Nigeria.

*Research interests:* electromagnetics, antennas, radiowave propagation, computational methods

*E-mail:* [amowete@unilag.edu.ng](mailto:amowete@unilag.edu.ng)

*ORCID:* <https://orcid.org/0000-0002-8335-6170>

---

## Физика волновых процессов и радиотехнические системы 2025, vol. 28, no. 2, pp. 24–39

DOI [10.18469/1810-3189.2025.28.2.24-39](https://doi.org/10.18469/1810-3189.2025.28.2.24-39)

УДК 621.396.674.3

Оригинальное исследование

Дата поступления 20 октября 2024

Дата принятия 21 ноября 2024

Дата публикации 30 июня 2025

## Сравнительный анализ криволинейных конфигураций антенны V-диполя


А.А. Айоринде , С.А. Адекола , И. Мовете 

Университет Лагоса  
Нигерия, Лагос,  
Юниверсити-роуд

**Аннотация – Обоснование.** Криволинейные дипольные антенные структуры были созданы как решение проблемы направленности, связанной с обычными дипольными антеннами, с длиной более половины длины волны. Однако, за исключением «вогнутого Nu» диполя, другие криволинейные конфигурации антенны V-диполя еще не получили аналитического внимания в открытой литературе. В этой статье представлен сравнительный анализ четырех таких конфигураций. **Цель.** Разработать подробную формулировку интегрального уравнения электрического поля для внутренней электродинамической задачи четырех криволинейных конфигураций структуры антенны V-диполя, чтобы метод решения моментов стал применимым. **Методы.** Неизвестные распределения тока в формуле определяются с помощью метода моментов с кусочно-линейным базисом и проверочными функциями. Аналитические результаты затем реализуются в компьютерной программе FORTRAN для численных результатов. **Результаты.** Аналитические модели для четырех криволинейных конфигураций V-дипольной антенны, а также результаты вычислений для их входных и радиационных характеристик. **Заключение.** Полученные результаты вычислений показывают, что с точки зрения максимально достижимой направленности и возвратных потерь наилучшими являются конфигурации с обоими изогнутыми плечами; за ними следуют обычные V, выпуклые Nu (одно плечо загнуто внутрь) и вогнутые Nu (одно плечо загнуто наружу).

**Ключевые слова** – криволинейная дипольная антенна; максимальная направленность; метод моментов; конфигурации антенн Nu-диполь; возвратные потери.

✉ amowete@unilag.edu.ng (Мовете Ике)

 © Айоринде А.А., Адекола С.А., Мовете И., 2025

## Список литературы

1. Landstorfer F. A new type of directional antenna // 1976 Antennas and Propagation Society International Symposium. 1976. P. 169–172. DOI: <https://doi.org/10.1109/APS.1976.1147636>
2. Landstorfer F.M. New developments in VHF/UHF antennas // International Conference on Antennas and Propagation. Proceedings. Part 1. 1978. P. 132–141.
3. Kataja J., Nikoskinen K. The parametric optimization of wire dipole antennas // IEEE Transactions on Antennas and Propagation. 2011. Vol. 59, no. 2. P. 350–356. DOI: <https://doi.org/10.1109/TAP.2010.2096181>
4. Junhong W., Lang R. Directivity optimization of curved surface dipole antennas // Journal of Electronics (China). 1994. Vol. 11, no. 4. P. 322–331. DOI: <https://doi.org/10.1007/BF02778386>
5. Jun-Hong W., Lang J. Analysis of curvilinear dipoles and their arrays with finite reflectors // Proceedings of IEEE Antennas and Propagation Society International Symposium and URSI National Radio Science Meeting. 1994. Vol. 2. P. 1002–1006. DOI: <https://doi.org/10.1109/APS.1994.407919>
6. Cheng D.K., Liang C.H. Shaped wire antennas with maximum directivity // Electronics Letters. 1982. Vol. 18, no. 19. P. 816–818. DOI: <https://doi.org/10.1049/el:19820555>
7. Liang C.H., Cheng D.K. Directivity optimization for Yagi-Uda arrays of shaped dipoles // IEEE Transactions on Antennas and Propagation. 1983. Vol. 31, no. 3. P. 522–525. DOI: <https://doi.org/10.1109/TAP.1983.1143085>
8. Chen W., Jen L., Zhang S.M. Radiation pattern optimisation for Yagi-Uda arrays of shaped dipole antennas // Electronics Letters. 1994. Vol. 30, no. 16. P. 1264–1265. DOI: <https://doi.org/10.1049/el:19940877>
9. Optimization of shaped wire antennas for asymmetric excitation / Z. Cai [et al.] // International Conference on Microwaves and Communications (ICMC). 1992. P. 316–319. URL: <https://www.ece.uvic.ca/~jbornema/Conferences/023-92icmc-cjbl.pdf>
10. Tang C. Input impedance of arc antennas and short helical radiators // IEEE Transactions on Antennas and Propagation. 1964. Vol. 12, no. 1. P. 2–9. DOI: <https://doi.org/10.1109/TAP.1964.1138164>
11. Miniaturized arc shaped near isotropic self-complementary antenna for spectrum sensing applications / U.U.R. Qureshi [et al.] // Sensors. 2023. Vol. 23, no. 2. P. 927. DOI: <https://doi.org/10.3390/s23020927>
12. Petković D.M., Krstić D.D. A new approach to V-dipole antenna // Facta Universitatis. Series: Working and Living Environmental Protection. 2002. Vol. 2, no. 2. P. 143–149. URL: <http://facta.junis.ni.ac.rs/walep/walep2002/walep2002-06.pdf>
13. Modeling nanoscale V-shaped antennas for the design of optical phased arrays / R. Blanchard [et al.] // Phys. Rev. B. 2012. Vol. 85, no. 15. P. 155457–1–11. DOI: <https://doi.org/10.1103/PhysRevB.85.155457>
14. Kim K., Scott W.R. Design of a resistively loaded vee dipole for ultrawide-band ground-penetrating radar applications // IEEE Transactions on Antennas and Propagation. 2005. Vol. 53, no. 8. P. 2525–2532. DOI: <https://doi.org/10.1109/TAP.2005.852292>
15. Mohamed A., Shafai L. Investigation on vee dipole antennas for ultra-wideband applications // 2009 13th International Symposium on Antenna Technology and Applied Electromagnetics and the Canadian Radio Science Meeting. 2009. P. 1–4. DOI: <https://doi.org/10.1109/ANTEMURSI.2009.4805093>
16. Wang J.H., Jen L., Jian S.S. Optimization of the dipole shapes for maximum peak values of the radiating pulse // IEEE Antennas and Propagation Society International Symposium. 1997. Vol. 1. P. 526–529. DOI: <https://doi.org/10.1109/APS.1997.630214>
17. Misra I., Chakrabarty R., Mangaraj B. Design, analysis and optimization of V-dipole and its three-element Yagi-Uda array // Progress in Electromagnetics Research. 2006. Vol. 66. P. 137–156. DOI: <https://doi.org/10.2528/PIER06102604>
18. Okereke O.U. Analysis of Nu-dipole antenna using the method of moments // International Journal of Electronics. 1999. Vol. 86, no. 12. P. 1481–1492. DOI: <https://doi.org/10.1080/002072199132563>
19. Табаков Д.П., Аль-Нозайли Б.М. Решение внутренней задачи для конечной регулярной двумерной решетки спиральных элементов, возбуждаемой плоской электромагнитной волной // Физика волновых процессов и радиотехнические системы. 2024. Т. 27, № 3. С. 17–33. DOI: <https://doi.org/10.18469/1810-3189.2024.27.3.17-33>

20. Sarkar T.K., Djordjevic A.R., Kolundzija B.M. Method of Moments Applied to Antennas. URL: <https://mtt.etf.bg.ac.rs/Mikrotalasna.Tehnika/Clanci/ANTMOM.pdf>
21. Harrington R.F. Matrix methods for field problems // Proceedings of the IEEE. 1967. Vol. 55, no. 2. P. 136–149. DOI: <https://doi.org/10.1109/PROC.1967.5433>
22. Kuo D.C., Strait B.J. Improved programs for analysis of radiation and scattering by configuration of arbitrarily bent wires // Syracuse University Scientific Report No. 15. 1972. 44 p. URL: <http://ece-research.unm.edu/summa/notes/In/0275.pdf>
23. Bird T.S. Definition and misuse of return loss [Report of the transactions editor-in-chief] // IEEE Antennas and Propagation Magazine. 2009. Vol. 51, no. 2. P. 166–167. DOI: <https://doi.org/10.1109/MAP.2009.5162049>
24. Balanis C.A. Antenna Theory: Analysis and Design. New Jersey: John Wiley & Sons, Inc., 1997. P. 543–546.
25. Burberry R.A. VHF and UHF Antennas. London: Peter Peregrinus Ltd., 1992. 312 p.

## Информация об авторах

**Айоринде Айотунде А.**, Ph.D. электротехника, старший преподаватель кафедры электротехники и электроники Университета Лагоса, Акока, Лагос, Нигерия.

*Область научных интересов:* электромагнетизм, антенны, распространение радиоволн, вычислительные методы.

*E-mail:* [aayorinde@unilag.edu.ng](mailto:aayorinde@unilag.edu.ng)

*ORCID:* <https://orcid.org/0009-0005-9731-8924>

**Адекола Сулейман А.**, Ph.D. электротехника, почетный профессор кафедры электротехники и электроники Университета Лагоса, Акока, Лагос, Нигерия.

*Область научных интересов:* электромагнетизм, антенны, распространение радиоволн, акустические (эхозондовые) антенны, сбор радиочастотной энергии.

*E-mail:* [adekolaadeniyi43@gmail.com](mailto:adekolaadeniyi43@gmail.com)

*ORCID:* <https://orcid.org/0000-0002-3926-5378>

**Мовете Ике**, Ph.D. электротехника, профессор кафедры электротехники и электроники Университета Лагоса, Акока, Лагос, Нигерия.

*Область научных интересов:* электромагнетизм, антенны, распространение радиоволн, вычислительные методы

*E-mail:* [amowete@unilag.edu.ng](mailto:amowete@unilag.edu.ng)

*ORCID:* <https://orcid.org/0000-0002-8335-6170>